Supplementary Information

Effects of laser photolysis of hydrocarbons at 193 and 248 nm on chemical vapor deposition of diamond films

Loic Constantin,[1,2,‡] Lisha Fan,[1,‡] Clio Azina,[1,2] Kamran Keramatnejad,[1] Jean-Francois Silvain,[1,2,] and Yong Feng Lu[1,*]*

[1]Department of Electrical and Computer Engineering, University of Nebraska, Lincoln, NE 68588, USA

[2]Institut de Chimie de la Matière Condensée de Bordeaux – ICMCB-CNRS 87, Avenue du Docteur Albert Schweitzer, F-33608 Pessac Cedex, France.

KEYWORDS: photolysis, ultraviolet laser, diamond, combustion chemical vapor deposition.

*Correspondences: Prof. Yongfeng Lu ; Address: Electrical and Computer Engineering Department, University of Nebraska-Lincoln, 209N Walter Scott Engineering Center, Lincoln, NE, 68588; Tel: 402-472-8323; Fax: 402-472-4732; Email: ylu2@unl.edu.

Prof. Jean-Francois Silvain: Address: Institut de Chimie de la Matière Condensée de Bordeaux – ICMCB-CNRS 87, Avenue du Docteur Albert Schweitzer, F-33608 Pessac Cedex, France. Email: silvain@icmcb-bordeaux.cnrs.fr

.

1. Experimental setup for flame chemistry analysis

The effects of ultraviolet (UV) laser irradiation on the combustion flame chemistry was analyzed by optical emission spectroscopy (OES), as illustrated in **Figure S1**. Two pulsed UV lasers were used, a krypton fluoride (KrF) excimer laser (Lambda Physik®, COMPex® 205, 248 nm, 20 ns) and an argon fluoride (ArF) excimer laser (Lambda Physik®, COMPex® 205, 193 nm, 15ns). Laser beams were focused to a size of about 7 × 4 mm^2 in the combustion flame using a 20 cm focal length UV lens. A spectrometer (Andor Technology, 3 gratings: 150, 600, 2400 l/mm; range: 190-800 nm) was synchronized with the laser by a digital delay generator (Stanford Research Systems DG 535, 5 ps delay resolution). A gate delay of 0 μs, a gate width of 10 μs, and a laser frequency of 35 Hz was used for all spectra and image acquisitions. Spectra and optical images were acquired over 500 pulses.

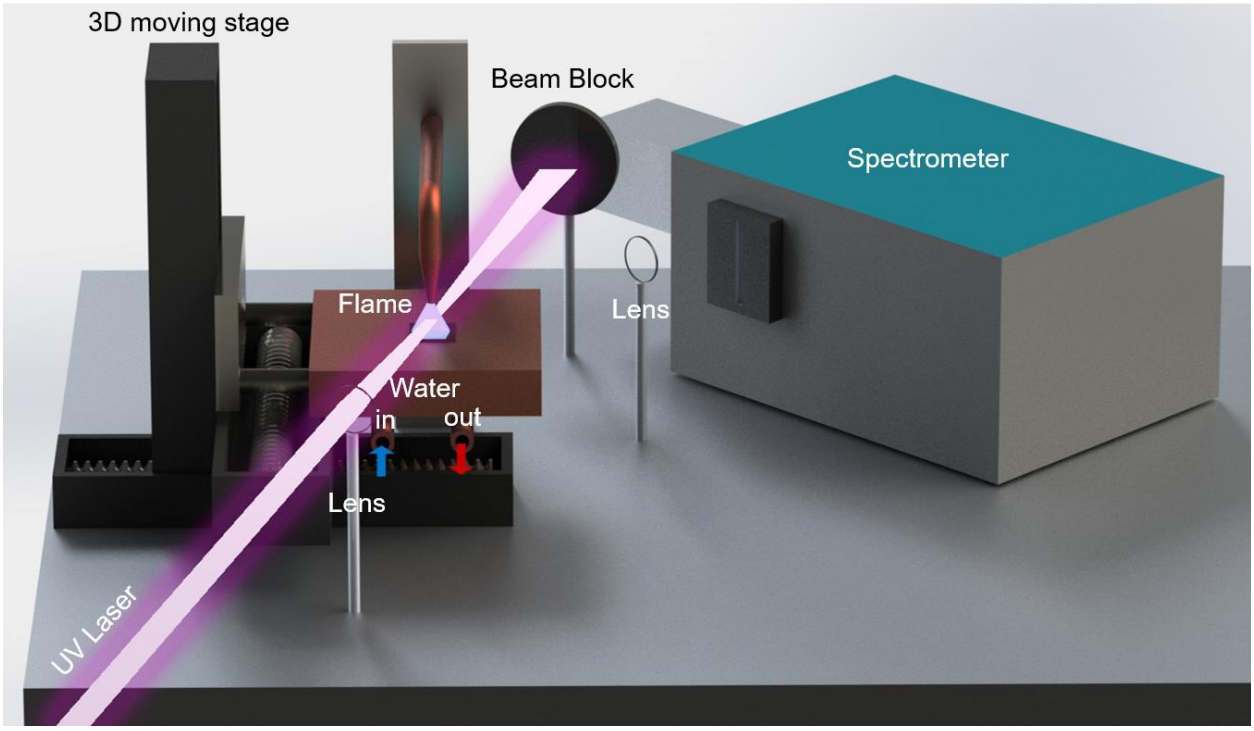

Figure S1. Schematic illustration of the experimental setup of UV-laser-assisted diamond CVD associated with the OES measurement.

2. Diamond thickness profiles and Raman spectra

Diamond growth rates were measured using a 3D surface profiler (ZYGO NewView™ 8300). Thickness profiles of diamond films prepared at different lasers fluences were retrieved from edge to edge on the substrates. **Figure S2** shows the measured thicknesses of the diamond films for both UV lasers at different fluences. The growth rate increased as the laser fluence increased, reaching 11 μm/h at a laser fluence of 25 mJ/cm^2 for the 193 nm laser and 10.3 μm/h at a laser fluence of 900 mJ/cm^2 for the 248 nm laser.

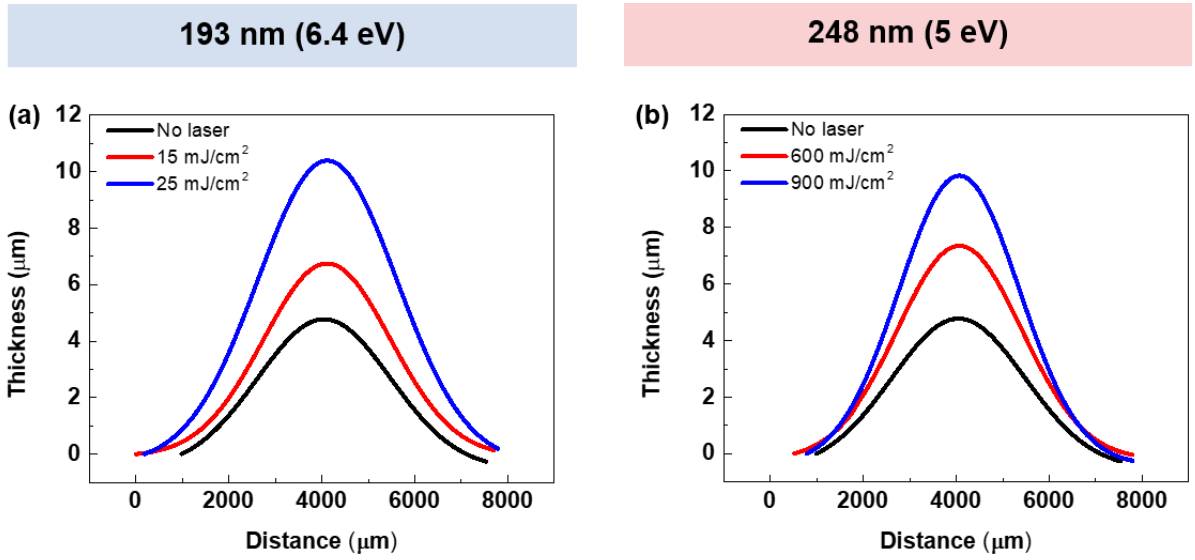

Figure S2. Thickness profiles of diamond films prepared at different laser fluences under (a) 193 and (b) 248 nm laser irradiations.

Diamond quality was evaluated using Raman spectroscopy. **Figure S3** shows Raman spectra of the diamond films prepared with 193 and 248 nm laser irradiations at different fluences. All spectra exhibited a diamond peak at 1332 cm^{-1} and two graphite bands at 1370 (D-band) and 1500 cm^{-1} (G-band). The diamond quality was evaluated by retrieving the quality factor index, Q_i = $I_{diamond}$ / ($I_{diamond}$ + $I_{a\text{-}carbon}$ / 233), where $I_{diamond}$ and $I_{a\text{-}carbon}$ are the integrated intensities of the diamond peak and the sum of the integrated intensities of the nondiamond carbon bands,

respectively. Nondiamond band intensities decreased as laser fluence increased, suggesting that the diamond quality was improved.

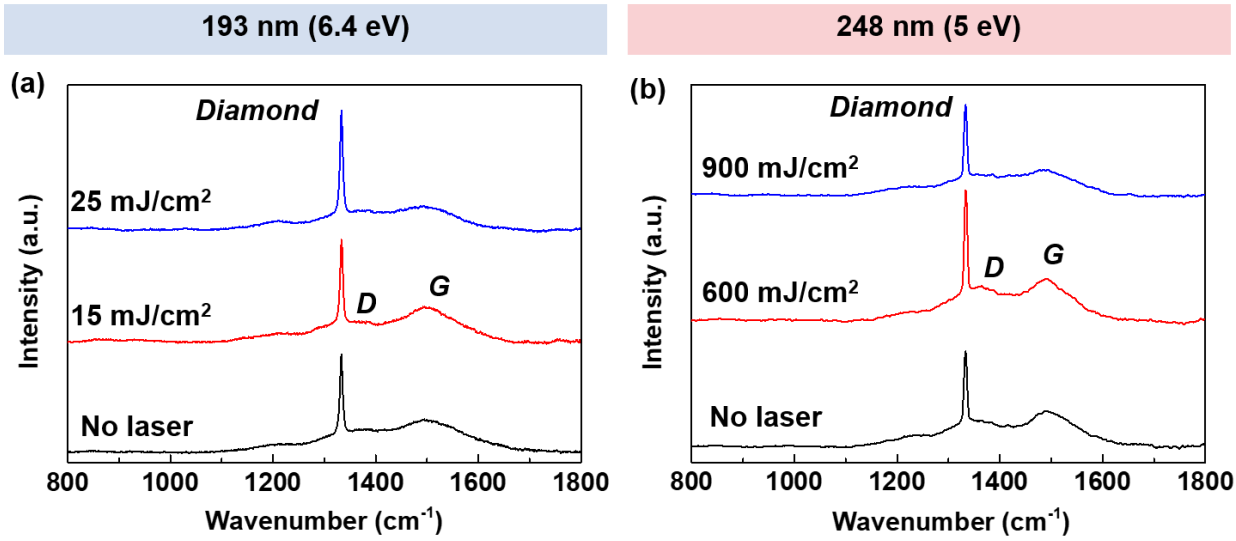

Figure S3. Raman spectra of the diamond films prepared with (a) 193 and (b) 248 nm laser irradiations at different laser fluences.

3. Cross-sectional microstructures of the diamond films

Diamond films were prepared at 193 and 248 nm for different laser fluences to study the effect of UV irradiation on the lateral grain size evolution. As shown in **Figure S4**, the UV lasers in both cases induced a faster lateral grain size evolution, which can be attributed to the suppression of secondary nucleation in the early stage of diamond deposition. However, the effect of the laser wavelength was not obvious.

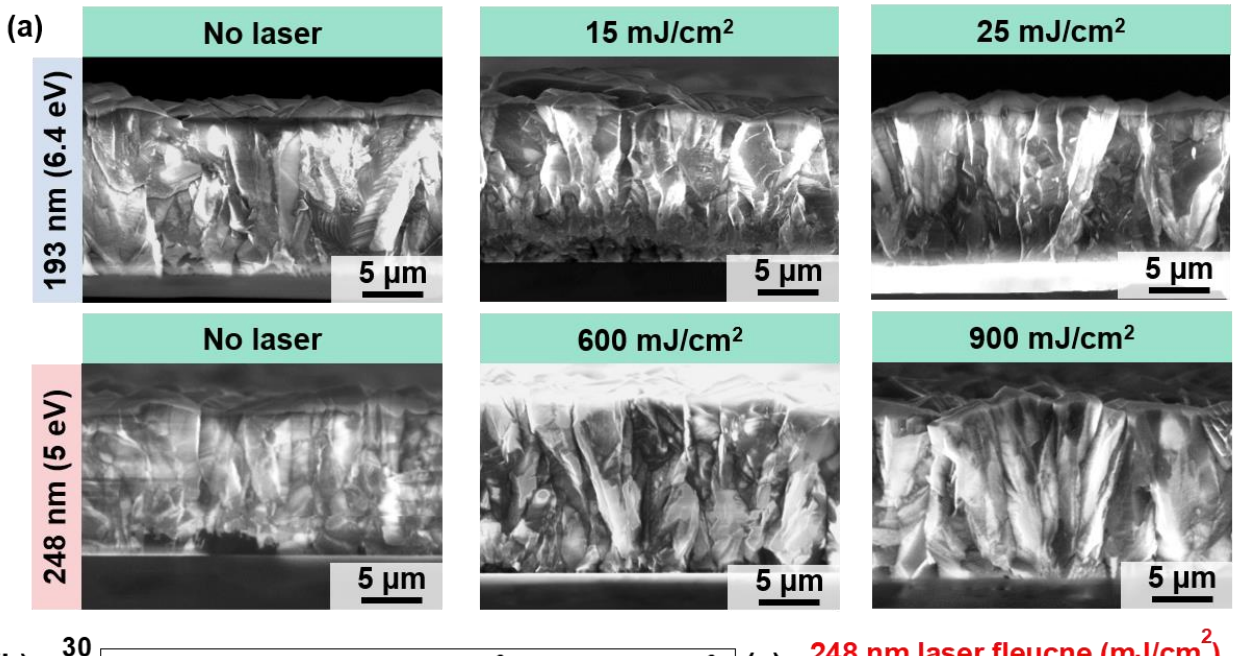

Figure S4. Cross-sectional SEM micrographs of the diamond films obtained under 193 and 248 nm laser irradiations at different laser fluences.

4. Experimental procedure of the diamond nucleation study

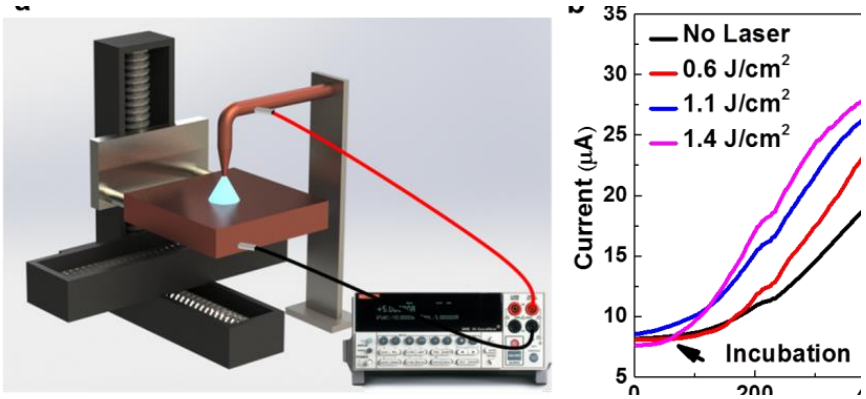

Figure S5. Schematic illustration of the experimental setup for *in situ* field-enhanced thermionic current measurement.

Diamond has a negative electron affinity, electrons can be emitted from diamond surfaces with little or no loss of energy. The electrons can be extracted from the surfaces simply by heating the diamond to temperatures above around 350°C. This 'boiling' off of electrons is known as 'thermionic emission'. During the diamond nucleation stage at a growth temperature of 800°C,

each diamond nucleus works as a tiny emitter, which contributes to a measurable thermionic emission current together. As the diamond nucleation proceeds, the thermionic current increases due to an increase in the number of diamond nuclei until the substrate surface is fully covered. Diamond nucleation was monitored in real time using the thermionic emission current. **Figure S5** shows the experimental setup *in situ* measuring the field-enhanced thermionic emission current. A power supply was connected to the flame torch and the brass sample holder. The bias voltage on the substrates was -5 V with respect to the flame torch. The current between the WC substrate and the torch was measured using a nano-ampere meter during the diamond growth.

5. Flame OES spectra and the flame temperature calculation procedure

Figure S6 shows OES spectra of the combustion flame under 193 and 248 nm laser irradiations at different fluences. Three main species were detected in all spectra: 1) C_2: $X'^3\Pi_u \leftarrow A^3\Pi_g$ (Δv = -1, 0, 1, 2); 2) CH: $A^2\Delta \leftarrow X^2\Pi$ ($\Delta v = 0$); and 3) OH: $A^2\Sigma^+ \leftarrow X^2\Pi$ ($\Delta v = 0$). Furthermore, the peaks of all species grew with respect to the laser fluence.

The flame temperature was approximately the rotational temperature derived from high-resolution rotational line emission intensities of CH, as shown in **Figures S7 (a) and (c)**. The Boltzmann plot was derived from the following equation:

$$\ln\left(\frac{I\lambda^4}{S_{J'J''}}\right) = -\frac{1}{T_r}\frac{E_{J'}}{k} + lnC$$

where I is the relative emission intensity of a rotational line obtained from the experimental spectrum, λ is the wavelength of the emitted spectral line, $S_{J'J''}$ is the rotational intensity factor, T_r is the rotational temperature, $E_{J'}$ is the rotational energy of the initial level, k is the Boltzmann constant, and C is a proportionality constant that is the same for all rotational transitions within a

band. **Figures S7 (b) and (d)** show the plots of $\ln(I\lambda^4/S_{J'J''})$ as functions of the $E_{J'}/k_B$, in which the slope is the inverse of the rotational temperature ($1/T_r$). All fitting curves resulted in very close slope values, implying comparable temperatures for all laser irradiation conditions.

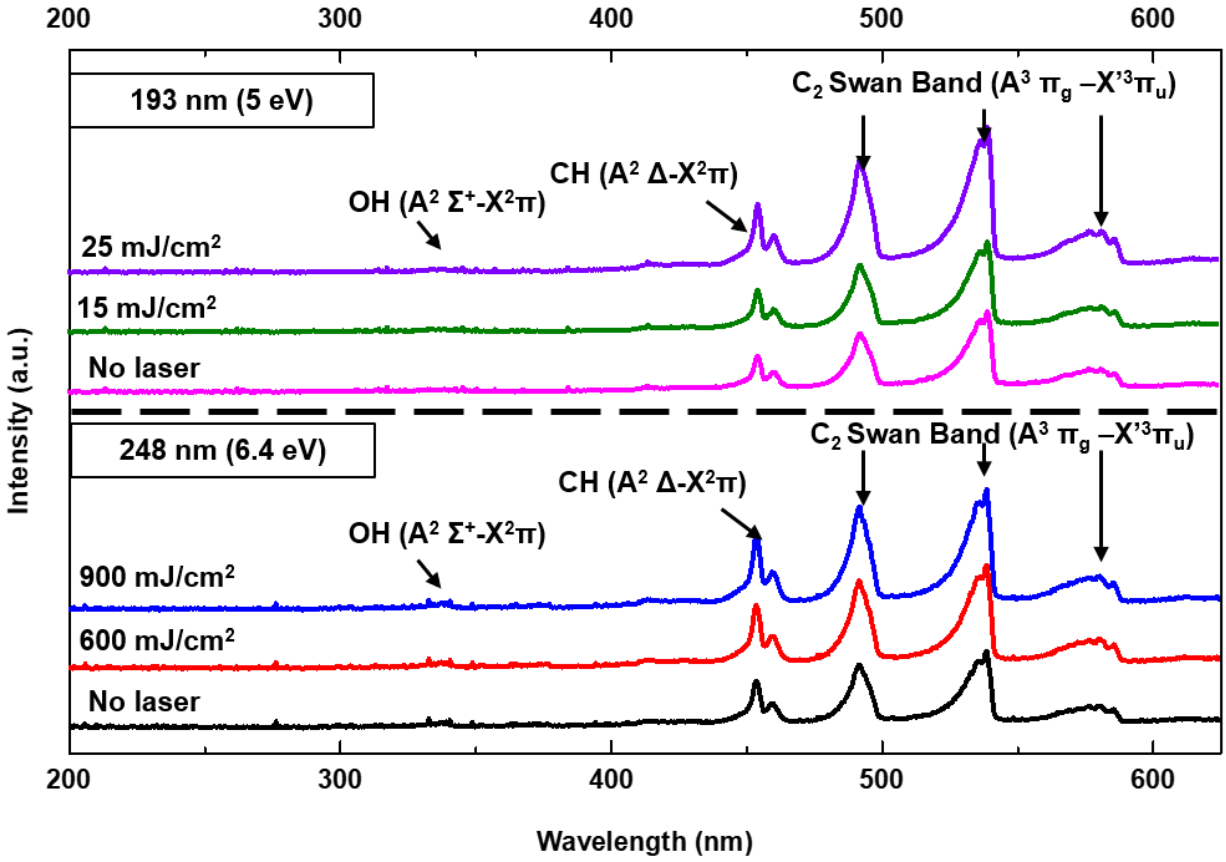

Figure S6. OES spectra of the combustion flame under 193 and 248 nm laser irradiations at different laser fluences.

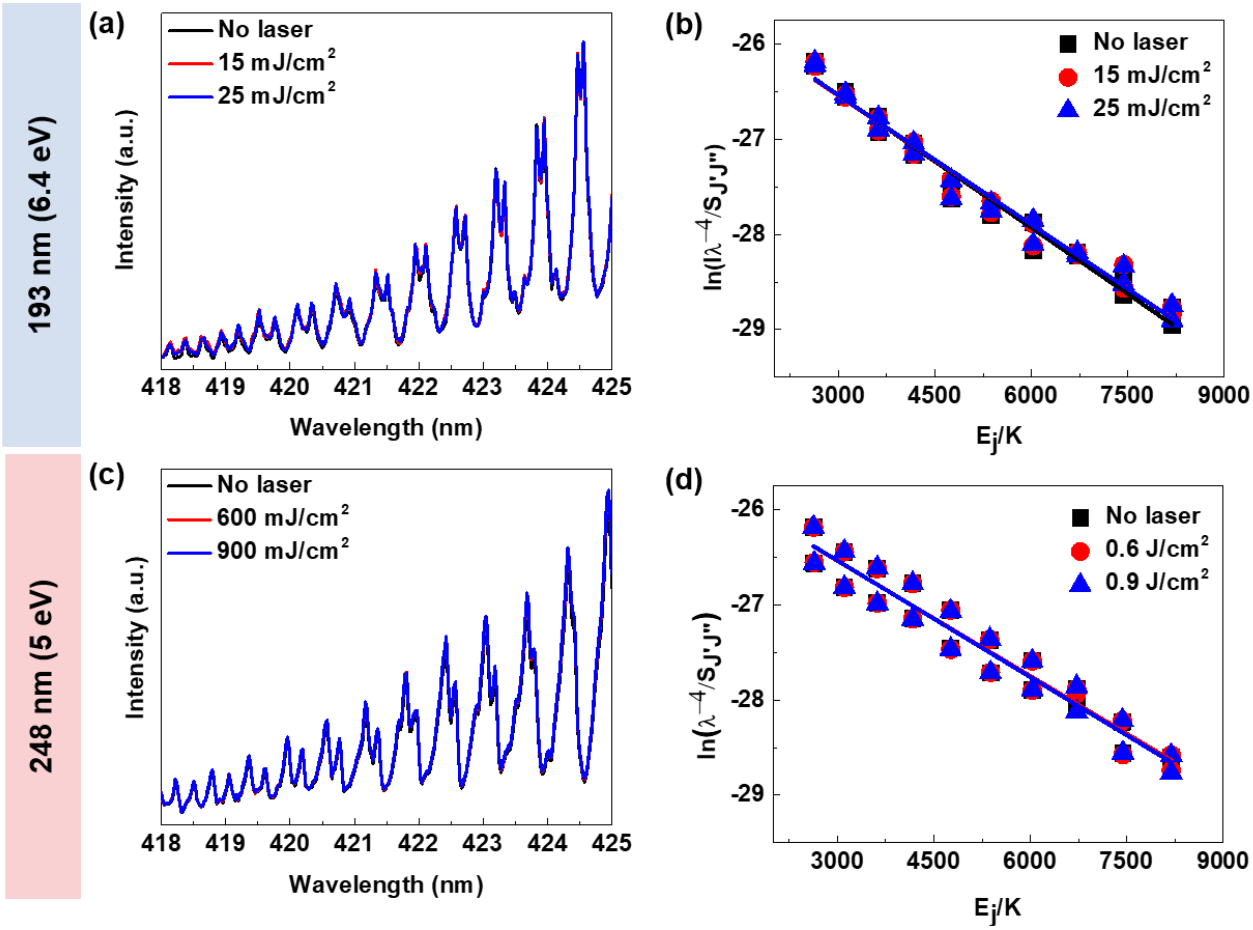

Figure S7. High-resolution optical emission spectra of the rotational R-branch of the CH and Boltzmann plots derived for flame temperature estimation of the combustion flame under (a-b) 193 and (c-d) 248 nm laser irradiations at different laser fluences.